Study of high-energy photoproduction with positron-annihilation radiation III. The reactions $\gamma p \to p 2\pi^+ 2\pi^- \pi^0$ and $\gamma p \to n 3\pi^+ 2\pi^-$

G. Alexander, O. Benary, S. Dagan, J. Gandsman, J. Grunhaus, A. Levy, and Y. Oren
Department of Physics and Astronomy, Tel-Aviv University, Ramat Aviv, Israel

J. Ballam, G. B. Chadwick, and M. M. Menke
Stanford Linear Accelerator Center, Stanford University, Stanford, California 94305

Y. Eisenberg, B. Haber, E. E. Ronat, A. Shapira, and G. Yekutieli
Weizmann Institute of Science, Rehovot, Israel
(Received 31 May 1973)

The reactions $\gamma p \to p 2\pi^+ 2\pi^- \pi^0$ and $\gamma p \to n 3\pi^+ 2\pi^-$ have been studied in three exposures of the SLAC 40-inch hydrogen bubble chamber to a positron-annihilation radiation of energies 4.3, 5.25, and 7.5 GeV. Cross sections for $\Delta^{++}(1236)$, ω, η, and ρ production are given. The associated production $\gamma p \to \Delta^{++}\omega^0\pi^-$ is discussed in terms of a double-Regge exchange model and compared with the reaction $\gamma p \to \Delta^{++}\rho\pi^-$.

I. INTRODUCTION

This is the third part of a final report on a photoproduction experiment carried out with the e^+e^- annihilation beam[1] in the SLAC 40-inch hydrogen bubble chamber. The exposure has been carried out at three mean annihilation photon energies of 4.3, 5.25, and 7.5 GeV, taking a total of 1.5 million pictures. The experimental details concerning these three exposures have been published elsewhere, together with our results on the three-prong events.[2] The results on the reaction

$$\gamma p \to p 2\pi^+ 2\pi^- \tag{1}$$

have been described in another paper[3] where the role of resonance production present in the reaction was discussed in some detail. In this work we present the analysis of the five-prong events leading to six nonstrange particles, namely,

$$\gamma p \to p 2\pi^+ 2\pi^- \pi^0 \tag{2}$$

and

$$\gamma p \to n 3\pi^+ 2\pi^- . \tag{3}$$

Experimental details and cross sections are given in Sec. II. Single- and associated-resonance production in reaction (2) are described in Secs. III and IV, respectively. Finally, reaction (3) is discussed in Sec. V.

II. CROSS SECTIONS

The presence of a neutral particle in the final state of reaction (2) and (3) leads to a one-constraint (1C) hypothesis in the annihilation-beam regions where the incoming-photon energy is known to within ±2.5% and to a 0C hypothesis in the bremsstrahlung regions. There exist two main sources of contamination in the fitted samples of reaction (2) and (3). The first is due to the assignment of a multineutral final-state bremsstrahlung event to a single neutral annihilation-photon hypothesis, and the second, a wrong-hypothesis assignment of an ambiguous event where the ionization information is not useful. In order to obtain a cleaner sample of events, we adopted here the procedure already utilized in our three-prong data,[2] namely, we imposed cuts on the confidence level (C.L.) of the fit and on the calculated missing mass (MM) of the outgoing neutral particle. We thus accepted an event as coming from an annihilation photon and belonging to reaction (2) if it yielded a 1C fit with C.L. > 0.5% and a missing-mass value of $-0.18 < \mathrm{MM}^2 < 0.10$ GeV^2. For reaction (3) we have used the same confidence-level criterion and a cut of $0.6 < \mathrm{MM}^2 < 1.2$ GeV^2 for the missing neutron mass. For the cross-section calculations a correction has been applied corresponding to the loss of events due to the MM and C.L. cuts.

The cross-section values for reactions (2) and (3) were obtained as in Refs. 2–4 with the well-known pair-production cross section. The cross sections are given in Table I and Fig. 1 and they are compared with the cross-section values reported earlier by the SBT and SB collaborations[4] using an almost monoenergetic polarized photon beam. A general agreement exists between the various experimental cross-section values, which for reaction (2) rise from threshold to a value of ~6.5 μb at about 6 GeV and then seem to level off. The cross-section values for reaction (3) level off somewhat sooner.

TABLE I. Cross sections obtained for reactions (2)–(8).

Reaction \ E_γ (GeV)	Cross section (μb) 3.7–4.7	4.7–5.8	6.8–8.2
$\gamma p \to p 2\pi^+ 2\pi^- \pi^0$	5.0 ± 0.6	6.4 ± 0.7	7.4 ± 0.8
$\gamma p \to n 3\pi^+ 2\pi^-$	2.0 ± 0.4	1.9 ± 0.6	2.4 ± 0.9
$\gamma p \to \Delta^{++} \pi^+ 2\pi^- \pi^0$	1.9 ± 0.6	2.1 ± 1.1	2.6 ± 0.9
$\gamma p \to p \omega \pi^+ \pi^-$ [a]	2.3 ± 0.6	1.6 ± 0.5	1.2 ± 0.4
$\gamma p \to p \eta \pi^+ \pi^-$ [a]	1.2 ± 0.6	1.2 ± 0.5	0.7 ± 0.4
$\gamma p \to p \rho^- 2\pi^+ \pi^-$	1.3 ± 0.4	2.5 ± 0.5	1.9 ± 0.7
$\gamma p \to p \rho^+ \pi^+ 2\pi^-$	1.6 ± 0.4	0.5 ± 0.3	1.2 ± 0.5
$\gamma p \to p \rho^0 \pi^+ \pi^- \pi^0$	0.3 ± 0.2	1.6 ± 0.6	2.2 ± 0.7
$\gamma p \to \Delta^{++} \omega \pi^-$	1.2 ± 0.7	0.6 ± 0.3	0.8 ± 0.5

[a] Corrected for unobserved decay modes.

The normalized cross-section values of the two reactions shown in Figs. 1(c) and 1(d) as functions of the photon energy, lie on a straight line in the log-log plot. A fit of the data to the expression

$$\sigma^* = \sigma \times (\text{flux/Lorentz-invariant phase space}) \propto E_\gamma^{-n}$$

yields a value of $n = 4.7 \pm 0.3$ and $n = 3.9 \pm 0.4$ for the reactions (2) and (3), respectively. These values compare favourably with the values $4.1 < n < 5.6$ obtained for $\pi^\mp p$, $K^\mp$, pp, and $\bar{p}p$ reactions leading to six particles in the final state.[5]

III. SINGLE RESONANCE PRODUCTION

A. $\gamma p \to \Delta^{++} \pi^+ \pi^- \pi^- \pi^0$

One of the characteristics of reaction (1) is the strong production of the $\Delta^{++}(1236)$ resonance with an almost constant cross section.[3] The same feature is also present in the reaction (2). The $p\pi^+$ invariant-mass distribution is shown in Fig. 2 where two combinations per event are present. These data were fitted to a linear combination of Breit-Wigner (BW) shape for the Δ resonance, Lorentz-invariant phase space (LIPS), and self-reflection of Δ, as well as reflections due to other resonances (ρ, ω) present in the data. The best fit, illustrated by the curve in Fig. 2, indicates that about 40% of reaction (2) proceeds via

$$\gamma p \to \Delta^{++} 2\pi^- \pi^+ \pi^0 \qquad (4)$$

at all the three photon energies under study here. The cross sections calculated for this reaction, which are given in Table I, are approximately independent of the photon energy. Here it should be noted that these cross-section values as well as other cross-section values given in Table I also include the contributions from the decay products of associate resonance production such as $\gamma p \to \Delta \omega \pi$ (see shaded area of Fig. 2).

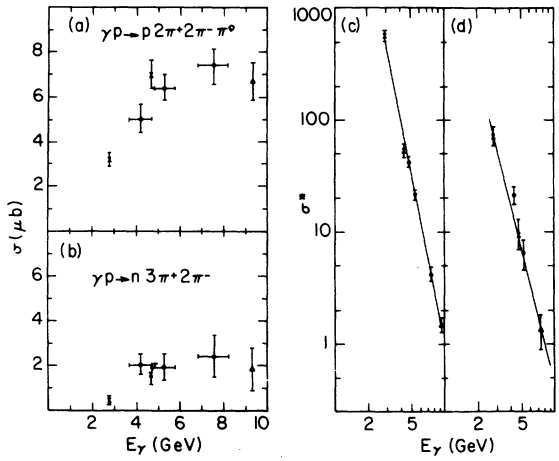

FIG. 1. Cross section and normalized cross sections: (a) and (c) for reaction $\gamma p \to p 2\pi^+ 2\pi^- \pi^0$; (b) and (d) for the reaction $\gamma p \to n 3\pi^+ 2\pi^-$. The full circles are from the present experiment; the crosses and triangles, respectively, are from the SBT and SB collaborations (Ref. 4).

B. $\gamma p \to p \omega \pi^+ \pi^-$ and $\gamma p \to p \eta \pi^+ \pi^-$

The $\pi^+ \pi^- \pi^0$ invariant-mass distributions for reaction (2) are shown in Fig. 3. The data were fitted to ω and η Gaussian-shaped resonances, their self-reflection, reflection of other resonances present in the data (Δ^{++}, ρ), and LIPS. The fits (solid lines in Fig. 3) yielded a total width of ~40 MeV for the ω and ~20 MeV for the η meson. The cross-section values for the reactions

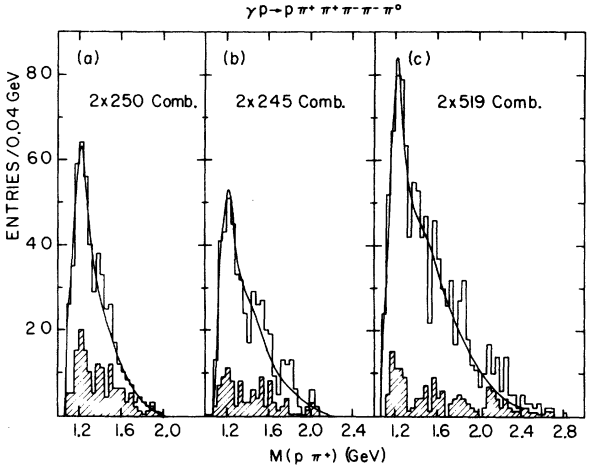

FIG. 2. $M(p\pi^+)$ distribution in the reaction $\gamma p \to p 2\pi^+ 2\pi^- \pi^0$ at three photon-energy intervals: (a) 3.7–4.7 GeV, (b) 4.5–5.8 GeV, and (c) 6.8–8.2 GeV. The curves represent the best fit to the data (see text). The shaded areas are the $p\pi^+$ combinations for which the other $\pi^+ \pi^- \pi^0$-mass combinations fall in the ω region $[0.74 < M(\pi^+ \pi^- \pi^0) < 0.83$ GeV].

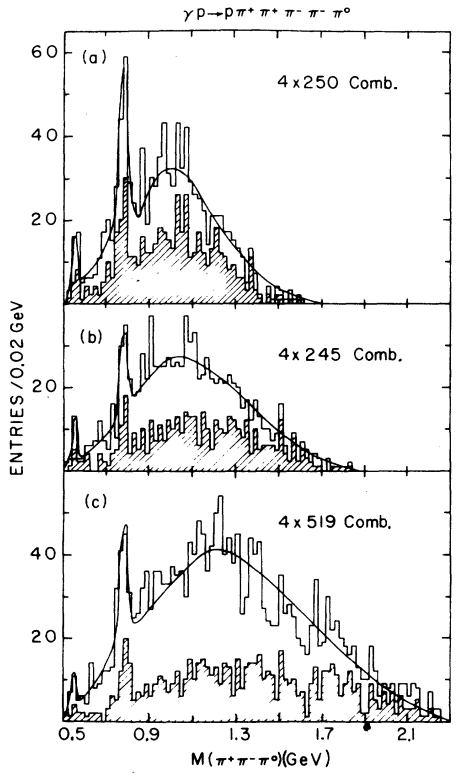

FIG. 3. $M(\pi^+\pi^-\pi^0)$ distribution in the reaction $\gamma p \to p2\pi^+2\pi^-\pi^0$ at three photon-energy intervals as defined in Fig. 2. The curves represent the best fit to the data (see text). The shaded areas are the $\pi^+\pi^-\pi^0$ combinations for which the other $p\pi^+$ is inside the $\Delta(1236)$-mass region $[1.15 < M(p\pi^+) < 1.35$ GeV].

$$\gamma p \to p\omega\pi^+\pi^- \tag{5}$$

and

$$\gamma p \to p\eta\pi^+\pi^- \tag{6}$$

are presented in Table I. These values are corrected for unobserved decay modes by the factor of 1/0.9 for the ω and 1/0.237 for the η production.[6] The values obtained in this work are in agreement with the previously reported results.[7-10] The shaded areas in Fig. 3 represent the $\pi^+\pi^-\pi^0$ combinations for which the remaining $p\pi^+$ invariant mass lies in the $\Delta^{++}(1236)$ mass region (1.15–1.35 GeV). These shaded histograms show that a substantial amount of the ω is produced in association with $\Delta^{++}(1236)$ (see also Sec. IV).

C. $\gamma p \to p\rho\pi\pi\pi$

Figure 4 shows the dipion mass distributions with negative, neutral, and positive charge combinations, respectively. After the removal of the ω events (shaded areas) an enhancement in the ρ-meson region is seen in all charge modes and in particular at the highest photon-energy interval, pointing to the presence of the reactions

$$\gamma p \to p\rho^\pm\pi^\mp\pi^+\pi^-$$

and (7)

$$\gamma p \to p\rho^0\pi^0\pi^+\pi^- .$$

To estimate the cross section for these reactions we have fitted the mass plots to a superposition of BW resonance shape, ρ^0 self-reflection, LIPS, and reflections of other resonances present in the data. The ω cut introduced in the data was introduced in the LIPS distributions.

Finally, we have searched for the presence of other bosons in reaction (2) decaying into more than three pions and, in particular, in the $2\pi^+2\pi^-$ and $\omega\pi$ combination. No obvious structure in the mass plots of these multipions systems have been observed and their distributions were found to be well-described by LIPS and the ρ and ω mesons. In addition, no evidence has been found in the data for the presence of baryon resonances other than the $\Delta^{++}(1236)$.

IV. ASSOCIATED RESONANCE PRODUCTION

The $p\pi^+$ and $\pi^+\pi^-\pi^0$ mass distributions in the reaction $\gamma p \to p2\pi^+2\pi^-\pi^0$ have been jointly fitted in order to estimate the amount of associate Δ^{++} and ω production through the reaction

$$\gamma p \to \Delta^{++}\omega\pi^- . \tag{8}$$

The cross-section values for this reaction using the results of the fit are given in Table I for the three annihilation-photon energies. A similar associated resonance production $\gamma p \to \Delta^{++}\rho^0\pi^-$ has been observed in the channel $\gamma p \to p2\pi^+2\pi^-$ which was analyzed in terms of a double-Regge model.[3,11] In that analysis the baryon-exchange contributions were neglected and the ρ-dominance model was assumed in the initial state. For comparison, we have used the same method outlined in Ref. 3 in order to carry out a double-Regge-type analysis for the reaction (8). Again neglecting the contribution from baryon exchanges, we were left with two possible multiperipheral diagrams (see Fig. 5) to which the events were assigned according to the longitudinal momenta P_L of the outgoing mesons. Events with $P_L(\omega) > P_L(\pi^-)$ were assigned to diagram A of Fig. 5 where the ω is coupled to the photon vertex, and events with $P_L(\omega) < P_L(\pi^-)$ were assigned to diagram B of Fig. 5 where the pion is coupled to the photon vertex.

In considering the relative importance of the ρ and ω components of the photon in the reaction γp

$\rightarrow \Delta^{++}\omega\pi^-$, we were guided by the experimental findings of the $\gamma p \rightarrow \rho^0 p$ and $\gamma p \rightarrow \omega p$ reactions.[12,13] In these reactions it has been observed that while the ρ production is strongly dominated by a diffractive process, even at relatively low energies, the ω production has a substantial contribution from a pion-exchange mechanism even at intermediate photon energies. Thus, in the case of the ω production in the reaction $\gamma p \rightarrow \Delta^{++}\omega\pi^-$ we have considered the contribution of the ρ as well as the ω components of the photon.

In performing the double-Regge calculations, following the procedure outlined in Ref. 3, we have considered at the $p\Delta^{++}$ vertex the exchange of the π and ρ trajectories for both diagrams A and B of Fig. 5. Note that conservation of G parity at each vertex in the multiperipheral diagrams implies that the π exchange is connected to the ω component of the photon, whereas the ρ exchange corresponds to the ρ component. At the photon vertex, we have used in each case two different possible exchange trajectories as is shown in Fig. 5.

The center-of-mass angular distributions of the outgoing particles of the reactions $\gamma p \rightarrow \Delta^{++}\omega\pi^-$ are shown in Fig. 5 (for both diagrams A and B where the data of the three annihilation-photon energies was added together). The angular distributions of the particles coupled to the incident photon and target proton served to estimate the free parameters present in the double-Regge amplitude.[11] The predictions of the double-Regge model are compared with the data by the continuous and dashed curves in Fig. 5. As seen from this figure, an adequate description of the data assigned to diagram A of Fig. 5 is obtained for the exchange pairs (f^0, π) and (π, ρ). For diagram B data the exchange pairs $(\rho, \pi)(A_2, \rho)$ and (π, ρ) are acceptable.

A comparison between $\gamma p \rightarrow \Delta^{++}\rho^0\pi^-$ and $\gamma p \rightarrow \Delta^{++}\omega\pi^-$ can be made if one assumes the ρ-dominance model for the first reaction and the ω-dominance model for the second. In this case it follows from this work and that of Ref. 3 that the exchange pairs describing the data of the two reactions are

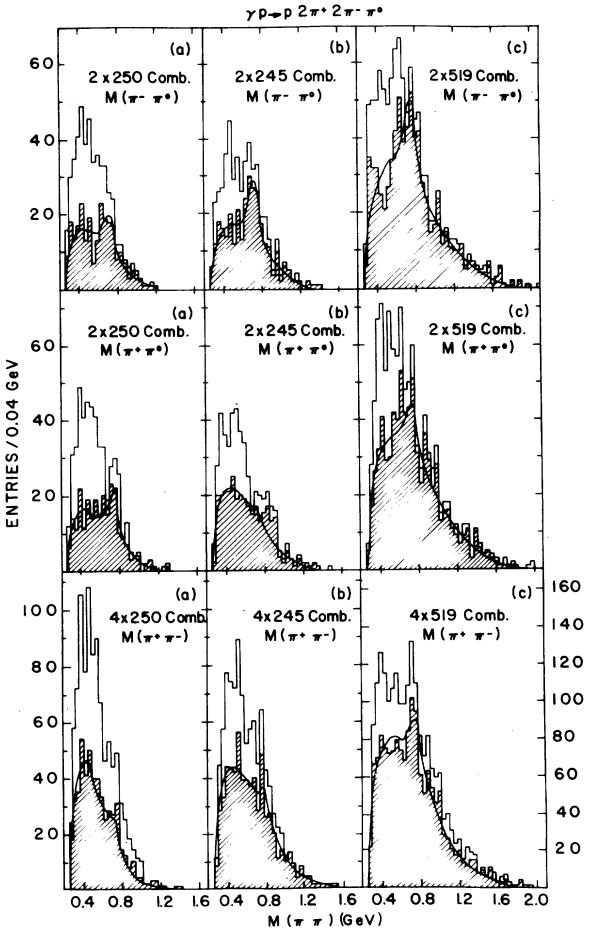

FIG. 4. The $M(\pi^-\pi^0)$, $M(\pi^+\pi^0)$, and $M(\pi^-\pi^+)$ distributions in the reaction $\gamma p \rightarrow p2\pi^+2\pi^-\pi^0$ at three photon-energy intervals: (a) 3.7–4.7 GeV, (b) 4.5–5.8 GeV, and (c) 6.8–8.2 GeV. The shaded areas correspond to $\pi\pi$ combinations after removing the ω-mass band. The curves represent the best fit to the shaded data (see text).

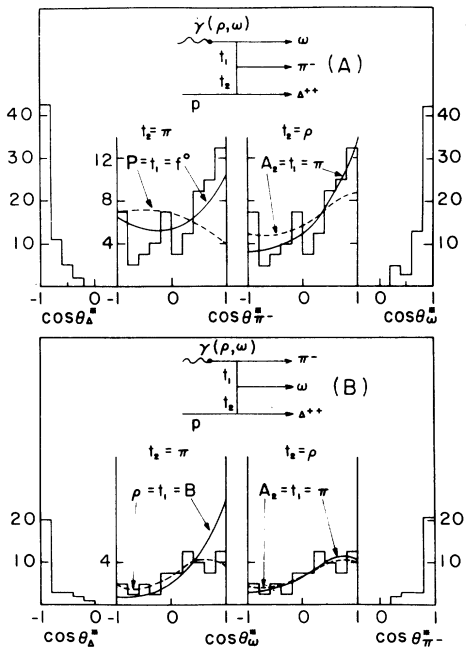

FIG. 5. Production angular distributions in the overall center-of-mass system for the outgoing particles, combining the data of all photon energies in the reaction $\gamma p \rightarrow \Delta^{++}\omega\pi^-$ assigned to either diagram A or diagram B. The solid and dashed curves represent the results of a double-Regge exchange model using several possible exchange trajectories (see text).

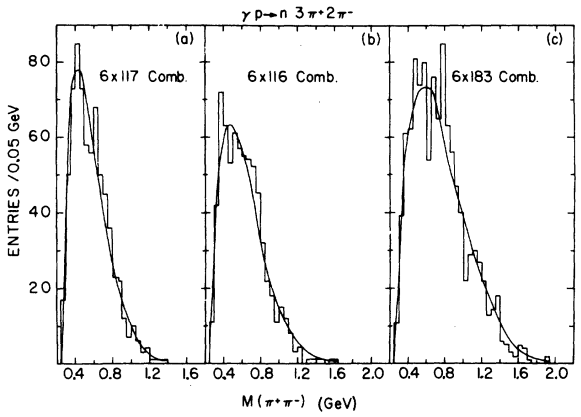

FIG. 6. $M(\pi^+\pi^-)$ distributions in the reaction $\gamma p \to n3\pi^+2\pi^-$ at photon energies: (a) 3.7–4.7 GeV, (b) 4.7–5.8 GeV, and (c) 5.8–8.2 GeV. The curves represent the LIPS predictions.

identical for diagram A of Fig. 5 and equal for diagram B in the framework of the exact exchange-degeneracy model, i.e., $(A_2, \pi) \equiv (\rho, \pi)$. The ratio of the cross sections $R = \sigma(\gamma p \to \Delta\rho\pi)/\sigma(\gamma p \to \Delta\omega\pi)$ is then essentially determined by the difference in values of the coupling constants in the two reactions. Since the dominant difference arises from the coupling of the photon to the ρ and the ω mesons, the expected value of R is ~9, whereas experimentally we find the value of ~2 for both diagrams A and B of Fig. 5. This disagreement suggests, therefore, that indeed both the ρ and the ω components of the photon contribute to the reaction $\gamma p \to \Delta\omega\pi$.

V. THE REACTION $\gamma p \to n3\pi^+2\pi^-$

In contrast to reactions (1) and (2), most of the reaction $\gamma p \to n3\pi^+2\pi^-$ features are adequately described by LIPS. This observation has already been noted for this reaction at lower energies.[7,8] Figure 6 illustrates the $\pi^+\pi^-$ mass distributions at the three photon energies of this experiment, where they are compared to the LIPS predictions. Although there is a general agreement with these predictions, one should remember that it would be very difficult to detect in the mass distributions a wide resonance due to the large combinatorial background. If one includes, nevertheless, in the mass fit a BW shape for the ρ resonance in addition to LIPS, one obtains ρ productions of $30 \pm 10\%$, $10 \pm 20\%$, and $50 \pm 20\%$ at the three photon energies, respectively. Consequently, one cannot exclude the presence of ρ meson in the data. Finally, in the $M(n\pi^\pm)$ distribution of reaction (3) no significant evidence for the presence of $\Delta^\pm(1236)$ was found.

ACKNOWLEDGMENTS

We wish to thank R. Watt and the 40-inch bubble chamber group as well as the SLAC operation crew for their assistance in performing this experiment. Our thanks are also due to Z.G.T. Guiragossian, P. Seyboth, and G. Wolf for their help during the early stages of the experiment.

[1]J. Ballam *et al.*, Nucl. Instrum. Methods 73, 53 (1969).
[2]Y. Eisenberg *et al.*, Phys. Rev. D 5, 15 (1972).
[3]G. Alexander *et al.*, Phys. Rev. D 8, 712 (1973).
[4]J. Ballam *et al.*, Phys. Rev. D 5, 545 (1972); H. H. Bingham *et al.*, *ibid.* 8, 1277 (1973).
[5]M. Muirhead and A. Poppleton, Phys. Lett. 29B, 448 (1969); T. Hofmokl and A. Wroblewski, *ibid.* 31B, 391 (1970).
[6]Particle Data Group, Phys. Lett. 39B, 1 (1972).
[7]Cambridge Bubble Chamber Group, Phys. Rev. 169, 1081 (1968).
[8]R. Erbe *et al.*, Phys. Rev. 188, 2060 (1969).
[9]J. Ballam *et al.*, Phys. Lett. 30B, 421 (1969).
[10]Y. Eisenberg *et al.*, Phys. Rev. Lett. 22, 669 (1969).
[11]G. Alexander *et al.*, Phys. Rev. 177, 2092 (1969).
[12]Cambridge Bubble Chamber Group, Phys. Rev. 146, 994 (1966); Aachen-Berlin-Bonn-Hamburg-Heidelberg-München Collaboration, Phys. Rev. 175, 1669 (1968).
[13]Y. Eisenberg *et al.*, Phys. Lett. 34B, 439 (1971).